

# Mutual control of critical temperature, RRR, stress, and surface quality for sputtered Nb films

E.V. Zikiy,<sup>1,2</sup> I.A. Stepanov,<sup>1</sup> S.V. Bukatin,<sup>1</sup> D.A. Baklykov,<sup>1,2</sup>  
M.I. Teleganov,<sup>1</sup> E.A. Krivko,<sup>1</sup> N.S. Smirnov,<sup>1</sup> I.A. Ryzhikov,<sup>1,3</sup>  
S.P. Bychkov,<sup>1</sup> S.A. Kotenkov,<sup>1</sup> N.D. Korshakov,<sup>1</sup>, J.A. Agafonova<sup>1</sup>  
and I.A. Rodionov<sup>1,2,\*</sup>

<sup>1</sup>FMN Laboratory, Bauman Moscow State Technical University, Moscow 105005, Russia

<sup>2</sup>Dukhov Automatics Research Institute (VNIIA), Moscow 127055, Russia

<sup>3</sup>Institute for Theoretical and Applied Electromagnetics RAS, Moscow 125412, Russia

\*email: [irodionov@bmstu.ru](mailto:irodionov@bmstu.ru)

## Abstract

Superconducting single quantum logic integrated circuits traditionally exploit magnetron sputtered niobium thin films on silicon oxide substrates. The sputtering depends on multiple process parameters, which dramatically affect mechanical, electrical, and cryogenic properties of Nb thin films. In this work, we focus on the comprehensive relationship study between 200-nm Nb film characteristics and their intrinsic stress. It is shown that there is a critical value of the working pressure  $p_{\text{critical}}$  at the fixed sputtering power above which stress in the film relaxes whereas the film properties degrade significantly. Below  $p_{\text{critical}}$  one can control intrinsic stress in the wide range from -400 MPa to +600 MPa maintaining perfect film surface with a 0.8 nm roughness (Rq), electrical resistivity less than 20  $\mu\Omega \times \text{cm}$ , critical superconducting transition temperature above 8.9 K and residual resistance ratio over 6.4. We suggest a modified kinetic model to predict Nb films stress with the linear dependence of high-energy parameters on the working pressure replaced with an exponential one, which allowed reduction of the approximation error from 20 to 8%.

## 1. Introduction

The key elements of single quantum logic (SFQ) circuits are Nb/Al/AIO<sub>x</sub>/Nb Josephson Junctions (JJ) and Nb-inductors, which are extremely promising for high-performance computing [1], [2], [3], [4] particularly as classical coprocessors for control and error tracking of large-scale quantum arrays [5], [6], [7], [8]. In addition, Nb/Al/Al/AIO<sub>x</sub>/Nb structures are the base of high-frequency receivers [9], parametric amplifiers [10], voltage standards [11], [12], and highly sensitive magnetic field sensors [13], [14]. The main material used in SFQ-circuits is thin-film niobium [15], [16], [17], which can also be used [18] to increase the quality of superconducting circuits [19]. There are many studies on magnetron sputtering parameters for the growth of high-quality polycrystalline Nb films evaluating the roughness [20], [21], intrinsic stress and roughness [22], [23], [24], residual resistance ratio (RRR) and intrinsic stress [25], critical

superconducting transition temperature ( $T_c$ ), and intrinsic stress [26], [27], [28]. But there is a work with comprehensive research [29], including joint analysis of intrinsic stress,  $T_c$  and critical current on Nb films sputtering parameters. However, an extensive study of the effect of magnetron sputtering parameters on the properties of niobium films on  $\text{SiO}_2$  for SFQ-circuits at room and cryogenic temperatures is still uncovered. We refer to these properties as roughness, intrinsic stress, electrical resistivity,  $T_c$ , and RRR.

Here we report a comprehensive study of the influence of magnetron sputtering parameters on the properties of niobium thin films on  $\text{SiO}_2$  and Nb-based structures at room and cryogenic temperatures. The relationship between the mechanical, electrical, and cryogenic properties of Nb films is demonstrated. We show that there is a critical value of the working pressure  $p_{\text{critical}}$  (3.0 mTorr in our case) at a fixed sputtering power, above which stress in the film relaxes but its properties degrade significantly. More than twenty 100-mm wafers with Nb films and 8 samples with Nb-structures are investigated, providing a wide range of experimentally measured 200-nm Nb-film properties. The results of the study provide a controllable intrinsic stress in 200-nm Nb-film in the range from compression 400 MPa to tensile 600 MPa maintaining perfect parameters of the films: roughness  $R_q$  less than 0.8 nm, electrical resistivity less than  $20 \mu\Omega \times \text{cm}$ , critical superconducting transition temperature more than 8.9 K and residual resistance ratio more than 6.4. A kinetic model of intrinsic stress generation is used to predict stress as a function of sputtering working pressure. An improvement of the kinetic model for high-energy methods of thin film deposition is proposed and allowed an approximation error improvement from 20 to 8%.

## 2. Experiments

100-mm silicon wafers with thermal 3- $\mu\text{m}$ -thick oxide on the surface are used as substrates for Nb thin films for room temperature characterization ( $\approx 305 \text{ K}$ ) of stress, electrical resistivity and roughness. Nb is deposited on  $25 \times 25 \text{ mm}$  3- $\mu\text{m}$   $\text{SiO}_2/\text{Si}$ -substrates to form Nb structures (Nb meanders with normal state resistance of 1 and 10 k $\Omega$  at room temperature and 4 and 2  $\mu\text{m}$  width) for cryogenic characterization of RRR and  $T_c$ . All of the deposition conditions are the same for different types of substrates. The wafers are not clamped in the holders, so they are deformed only by the intrinsic stress in the films. Substrates are cleaned with megasonic cleaning and Piranha solution (mixture of  $\text{H}_2\text{SO}_4$  and  $\text{H}_2\text{O}_2$ ) before deposition. Thin 200-nm Nb films are deposited in an ultrahigh vacuum magnetron sputtering system with 3" guns and with the base pressure below  $5 \times 10^{-9} \text{ mBar}$  as in ref [30]. The working pressure of argon  $p_{\text{Ar}}$  is varied from 0.3 to 7.0 mTorr, and the sputtering power  $P_{\text{sput}}$  is varied from 250 to 400 W. Substrate heating for Nb deposition is not allowed for the SFQ circuits [23], [31], so we cannot use our approaches to form ultra-smooth films [32], [33], all films are deposited at  $20^\circ\text{C}$ . The processing of the Nb structures on 25-mm substrate is done using  $\text{CF}_4$  plasma-based ICP RIE etching. The chip for cryogenic characterization is cut into  $10\text{mm}^2$  dies prior to measurements.

The electrical resistivity  $\rho_{\text{Nb}}$  of Nb films is measured at 64 points on the entire 100-mm wafers using the 4-probe method. This parameter is important, because according to the Mayadas–Shatzkes' grain boundary scattering model, an increase in resistivity indicates structural defects in the film [34]. Low surface roughness is critical for the uniform tunneling current in the Nb/Al/AlOx/Nb JJ [35]. We measured  $R_q$  at 25 points

across the entire wafer using a stylus profiler. Intrinsic stress in the films is measured, as high stress values result in a decrease of both Nb/Al/AlOx/Nb JJ' critical current reproducibility [22] and the  $R_{SG}/R_N$  quality factor of Josephson junctions [26]. The stress is calculated from the change in wafer curvature after the deposition of the Nb film. The initial and final wafer curvature is determined using a stylus profiler. High-resolution SEM images are acquired for all Nb films to measure the grain size.

For cryogenic characterization, the samples are cooled down using a pulse tube cryocooler at a base temperature of 2.5 K. For Nb structures, the RRR and  $T_C$  are measured with an accuracy of  $\pm 0.05$  K. RRR and  $T_C$  represent the quality of the thin film material structure (defects, grain boundaries). RRR is calculated as the ratio of the resistance of the Nb structure at 300 K and 10 K measured with the four-probe method. A direct relationship between RRR and the energy relaxation time  $T_1$  is demonstrated [36]. An inverse relationship between  $T_C$  and the number of structural defects has been shown for quantum superconducting circuits with a Nb base layer [29].

### 3. Results

#### 3.1 Surface and electrical film parameters as dependence on sputtering parameters

The main magnetron sputtering parameters are the working pressure  $p_{Ar}$  and sputtering power  $P_{sput}$ ; therefore, we studied the influence of these parameters on the properties of Nb films. Figure 1,a shows the dependence of Nb film roughness on  $p_{Ar}$ . At  $p_{Ar}$  less than 3 mTorr, the average roughness  $R_q$  on a 100-mm wafer does not exceed 8 Å, but the higher  $p_{Ar}$  results in a dramatic increase in  $R_q$  up to 18 Å. Figure 1,c shows the dependence of the resistivity of Nb films on  $p_{Ar}$  at the fixed  $P_{sput}$  of 400 W, from which it can be seen that both the resistivity  $\rho_{Nb}$  of the films and the variation ( $3\sigma$ ) of  $\rho_{Nb}$  values across the wafer increase at  $p_{Ar}$  greater than 2.0 mTorr. The  $P_{sput}$  in the range of 250 – 400 W had no significant effect on the  $\rho_{Nb}$  and roughness of Nb films.

The effect of  $P_{sput}$  at a fixed  $p_{Ar}$  of 1.0 mTorr on the stress in Nb films is shown in Figure 1,d. As  $P_{sput}$  increases, the stress becomes more compressive, but the effect of  $P_{sput}$  is small compared to the effect of  $p_{Ar}$ , as shown in Figure 1,e. As  $p_{Ar}$  increases from a minimum value of 0.3 mTorr, the stress changes from compressive to tensile. At a  $p_{Ar}$  value around 3.0 mTorr, which we named  $p_{critical}$ , the stress begins to decrease from the maximum tensile value. Figure 1,f shows the stress map for the Nb film with stress values ranging from -170 to 70 MPa and a wafer average of 25 MPa.

A well-known issue of magnetron sputtering is a target erosion effect on the film properties, including film stress. There are a number of methods to control stress in Nb thin films which have been studying for many years. Imamura et al. [29] proposed cathode voltage as a universal magnetron sputtering parameter to control the stress. However, Booi et al. [37] showed that the stress - cathode voltage relationship changes during target erosion and proposed to control the ratio of cathode current  $I_C$  and  $p_{Ar}$  to maintain stress value constant. Then Amos et al. [38] showed that the stress for the  $I_C/p_{Ar}$  ratio changes with target erosion and proposed to experimentally detect a single point on the  $p_{Ar}$ - $I_C$  plane that provides zero stress during the entire lifetime of the target. Modern magnetron power supplies allow a constant power mode, and it is reported in [39] that this mode provides stability of the stress during target erosion.

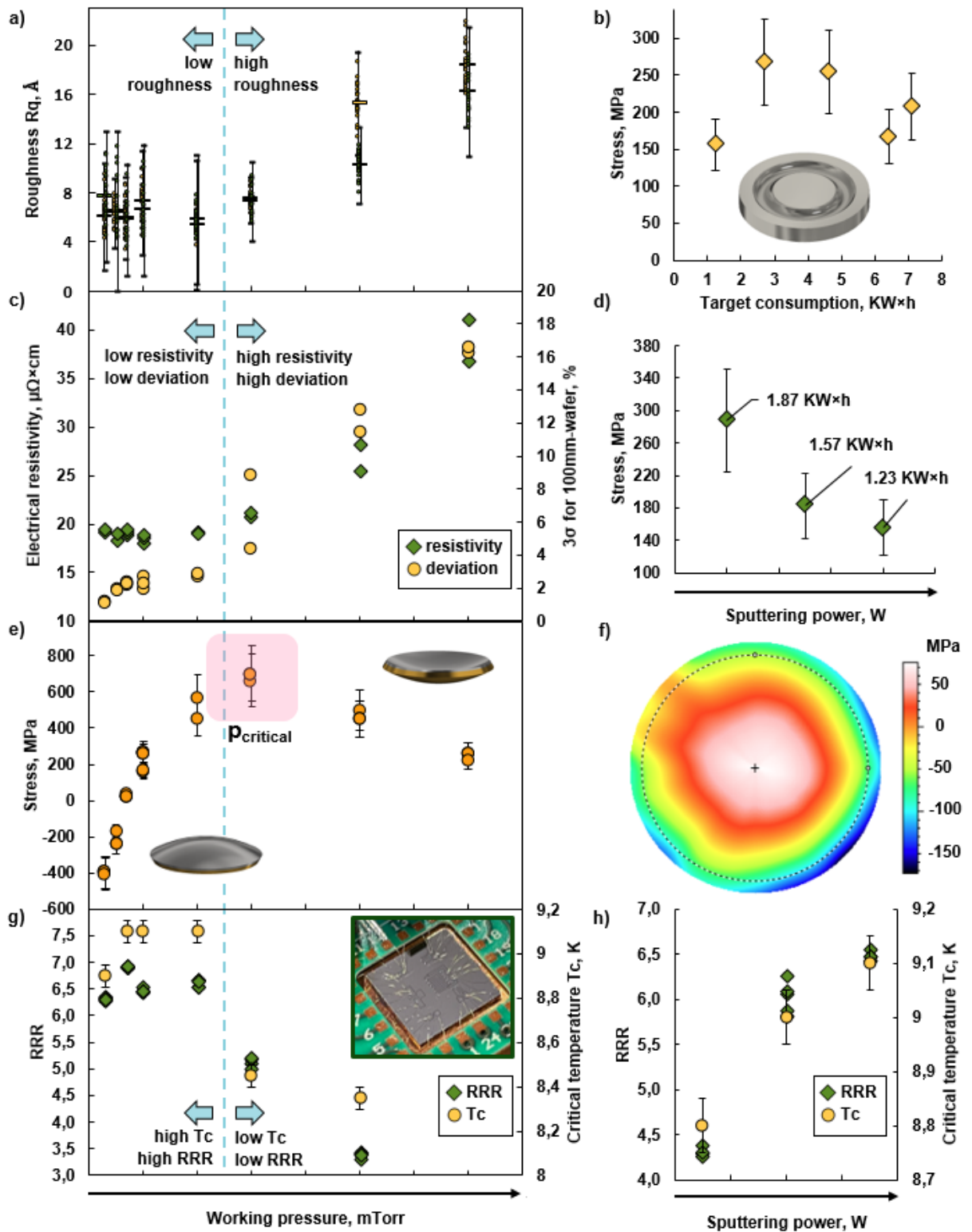


Figure 1. (a) Nb-films roughness  $R_q$  on a 100-mm wafer versus working pressure  $p_{Ar}$  (green and yellow points next to each other indicate two different wafers with identical films). (b) Stress in Nb films as a function of magnetron target lifetime. (c) The electrical resistivity average value and scatter ( $3\sigma$ , %) on a 100-mm wafer of Nb films versus the  $p_{Ar}$ . (d) Stress in Nb-films as a function of sputtering power  $P_{\text{sput}}$ . (e) Stress in Nb-films as a function of the  $p_{Ar}$ . (f) Example of a map of stress distribution on a 100-mm wafer. (g) RRR and  $T_c$  of Nb structures versus the  $p_{Ar}$  during the deposition of Nb films; the inset shows a photograph of a 10×10 mm chip for cryogenic characterization. (h) RRR and  $T_c$  Nb structures versus the  $P_{\text{sput}}$  during the deposition of Nb films.

We measured the stress of our Nb films deposited at  $P_{\text{sput}} 400 \text{ W}$  and  $p_{\text{Ar}} 1.0 \text{ mTorr}$  at target consumption from 1 to 7  $\text{kW}\times\text{h}$  (target resource 10  $\text{kW}\times\text{h}$ ) and found a slight and non-monotonic change in the stress, as shown in Figure 1,b. Thus, the fixation of  $P_{\text{sput}}$  and  $p_{\text{Ar}}$  ensures the stability of the stress throughout the target lifetime.

### 3.2 $T_C$ and RRR film parameters as dependence on sputtering parameters

The cryogenic properties of Nb films are investigated using a 4-probe method by measuring the voltage on Nb structures with room temperature resistance of 1 and 10  $\text{k}\Omega$ . An electrical connection of the test chip in the holder is shown in the inset of Figure 1,g. The dependence of the RRR and  $T_C$  of the Nb structures on  $p_{\text{Ar}}$  at a fixed  $P_{\text{sput}}$  of 400 W is shown in Figure 1,g. Each point on the plot refers to one structure on the chip.  $T_C$  and RRR decrease significantly at  $p_{\text{Ar}}$  greater than some  $p_{\text{Ar}}$ . The dependence of RRR and  $T_C$  of Nb structures on  $P_{\text{sput}}$  at a fixed  $p_{\text{Ar}}$  of 1.0 mTorr is shown in Figure 1,h.  $T_C$  and RRR increase monotonically with increasing  $P_{\text{sput}}$ , which is consistent with the data of [25].

### 3.3 Kinetic model for stress prediction in Nb films

Prediction of a thin films stress depending on the deposition parameters is an important problem as it plays a significant role in the reliability, reproducibility and functionality of thin film devices [40], [41], [42]. To the date, the stress formation in thin films is best described by the kinetic model [40], [43], [44]. We suggested a modification of the kinetic model for high-energy methods, in particular, magnetron sputtering [45], [46]. It is capable predicting the change of intrinsic film stress as a function of its thickness. However, in our experiment the stress is measured *ex situ* in a fully-formed film. Therefore, it is assumed that the stress is uniform over the film thickness. In this case, the final expression for the full stress in the film is

$$\begin{aligned} \sigma_{ss}^{\text{sputt}} &= \sigma_{\text{growth}} + \sigma_{\text{gb}}^{\text{energetic}} + \sigma_{\text{bulk}}^{\text{energetic}} \\ &= \left[ \sigma_C + (\sigma_T - \sigma_C) e^{-\frac{\beta D_{\text{eff}}}{RL}} \right] + A_0 \left( \frac{l_0}{L} \right) + \left( 1 - \frac{l_0}{L} \right) \frac{B_0}{\left( 1 + \frac{l_0}{RT_s} \right)}, \end{aligned} \quad (1)$$

where  $\sigma_{\text{growth}}$  is the stress resulting from the formation and densification of grain boundaries.  $\sigma_{\text{gb}}^{\text{energetic}}$  is compressive stress resulting from the densification of grain boundaries due to exposure of high-energy particles.  $\sigma_{\text{bulk}}^{\text{energetic}}$  is compressive stress resulting from the generation in the grain bulk and annihilation on the free surface of point defects due to exposure of high-energy particles.  $\sigma_C$  is compressive stress created by the insertion of adatoms into grain boundaries under the effect of non-equilibrium chemical potential at the surface (fitting parameter).  $\sigma_T$  is the tensile stress resulting from the formation of new segments of grain boundaries (fitting parameter).  $\beta D_{\text{eff}}$  is an exponential term describing the efficiency of diffusion of adatoms from the free surface into the grain boundaries (fitting parameter).  $R$  is the growth rate of the grain, i.e., the deposition rate of the film.  $L$  is the average grain size.  $l_0$  is the depth of defect generation by a high-energy particle in the grain bulk and the width of the grain boundary region where direct densification occurs under the effect of a high-energy particle (fitting

parameter).  $A_0$  is a fitting parameter that defines  $\sigma_{gb}^{energetic}$ .  $B_0$  is a fitting parameter that defines  $\sigma_{bulk}^{energetic}$  and directly proportional to the defect generation rate in the grain bulk under high-energy exposure. The next explicit dependence on the working pressure  $p$  is introduced for the parameters  $A_0$ ,  $B_0$ , and  $l_0$ :

$$A_0 = A^* \left(1 - \frac{p}{p_0}\right), \quad (2)$$

$$B_0 = B^* \left(1 - \frac{p}{p_0}\right), \quad (3)$$

$$l_0 = l^* \left(1 - \frac{p}{p_0}\right), \quad (4)$$

where  $p_0$  is some pressure value that is the same for all experiments in which only  $p$  is varied.  $A^*$ ,  $B^*$ ,  $l^*$  are fitting coefficients included in linear dependence of  $A_0$ ,  $B_0$ , and  $l_0$  on  $p$ . They reduce the total number of fitting parameters for a large number of experiments with different  $p$ .

$\tau_S$  is the characteristic time required for diffusion of a point defect from the grain bulk to the free surface and is determined by the expression:

$$\tau_S = \frac{l_0}{R} \left[ \alpha - 1 - \alpha \sqrt{1 - \left(\frac{2}{\alpha}\right)} \right], \quad (5)$$

where  $\alpha = \frac{D_i}{2Rl_0}$  for  $\alpha > 2$  and  $\alpha = 2$  for  $\alpha \leq 2$ , where  $D_i$  is the defect diffusion parameter (fitting parameter). When  $\alpha \leq 2$  all defects remain in the grain bulk.

The kinetic model can consider [47] the effect of the transverse grain size variation on the stress [48]. However, because our deposition regime is in zone I of the Thornton diagram [49], the transverse grain size can be considered constant over the entire grain height, similar to molybdenum films [50]. In the case of low melting point metals, relaxation of the intrinsic stress occurs after the thin film deposition, but for refractory metals, the level of stress is maintained [51]. Therefore, we consider that the stress we measured is equal to the stress immediately after Nb-deposition.

We approximated our experimental data on  $p_{Ar}$  - dependent stress using the non-linear least squares fitting routine. The values of stress (average), working pressure, grain size, and deposition rate used for fitting are presented in Table 1. The grain size  $L$  is defined as the diameter of a circle with a length equal to the perimeter of the grain in the SEM image. Due to the extremely low contrast, the grain boundary is traced manually. The grain size dependence of the Nb film on  $p_{Ar}$  is shown in Figure 2,a. SEM images of the Nb films deposited at  $p_{Ar}$  0.3, 0.7, 3.0, and 7.0 mTorr are shown in Figures 2,b, 2,c, 2,d, and 2,e, respectively. In Figure 2,f and Figure 2,g, the grain size  $L$ , nm is calculated as a linear function of the working pressure  $p$ , mT:

$$L = 2.7287 \times p + 47.95. \quad (6)$$

In model plots, the deposition rate  $R$ , nm/s is calculated as a linear function of the working pressure  $p$ , mT:

$$R = -0.0006 \times p + 0.2898. \quad (7)$$

Table 1. Input experimental data for the kinetic model.

№	Stress, GPa	$p_{Ar}$ , Pa	L, nm	R, nm/s
1	-0.400	0.0399	48.1	0.290
2	-0.203	0.0665	49.8	0.290
3	0.028	0.0931	49.4	0.290
4	0.211	0.1330	51.6	0.288
5	0.511	0.2660	52.5	0.288
6	0.681	0.3990	54.6	0.287
7	0.476	0.6650	66.4	0.287
8	0.242	0.9310	64.5	0.286

The published fitting parameter values for refractory materials are summarized in Table 2 along with the assumed value bounds and the starting values for the fitting parameters.

Table 2. Values of fitting parameters of the kinetic model from the literature and their fitting starting values and bounds.

ref.	film	dep.	$\sigma_t$ , GPa	$\sigma_c$ , GPa	$P_0$ , Pa	$\beta D_{eff}$ , nm <sup>2</sup> /s	$D_i$ , nm <sup>2</sup> /s	$A^*$ , GPa	$B^*$ , GPa	$l^*$ , nm
[45]	Mo	DC	4.24	-1.6	0.83	0.28	7.2	-167	-53.1	1.7
[45]	Mo	HiPIMS	4.24	-1.6	0.83	1.29	7.2	-115.2	-243	1.8
[46]	Mo	DC	0.78	-29.9	0.67	0.03	0.68	-2.60	-12	0.7
[52]	W	DC	3.16	-4	0.52	6e-9	0.24	-8.13	-11.57	0.62
[53]	Ti	Evap	1.08	-0.16	-	1.87	-	-	-	-
Start	Nb	DC	2	-20	0.6	0.03	0.6	-3	-12	0.8
Min	Nb	DC	0.5	-40	0.13	0	0	-10	-15	0.5
Max	Nb	DC	8	-1	1	1	10	0	0	4

Figure 2,f demonstrates the model fitting for the 8 experimental points (orange line). The model predicts an extremum in stress, as well as the experimental data. However, the model predicts that the stress will become increasingly compressive with further  $p_{Ar}$  increasing, but it was shown before [29], [22], [54], that it should relax to zero. If the first 6 points only are used for model fitting (without 5.0 and 7.0 mTorr points), the model also predicts a compression stress transition (orange line in Figure 2,g). The reason for this is the linear dependence of the parameters  $A_0$ ,  $B_0$ , and  $l_0$  on the working pressure. In this case, these parameters, corresponding to the effect of high-energy exposure on the stress in the film, are the same over the entire range of  $p$ . However, it is reasonable to assume that when some  $p$  is exceeded, the excess energy of the deposited atoms and “fast neutrals” is dissipated before reaching the substrate. Therefore, we

suggest replacing the linear dependence of the parameters  $A_0$ ,  $B_0$ , and  $l_0$  on  $p$  with an exponential ones:

$$A_0 = A^* \times p^* \left(\frac{p}{p_0}\right), \quad (8)$$

$$B_0 = B^* \times p^* \left(\frac{p}{p_0}\right), \quad (9)$$

$$l_0 = l^* \times p^* \left(\frac{p}{p_0}\right), \quad (10)$$

where  $p^*$  is a dimensionless exponential fitting parameter less than 1.0. In this case the effect of the parameters  $A_0$ ,  $B_0$ , and  $l_0$  on the stress decreases as  $p$  increases and asymptotically tends to zero. Figure 2, g shows in green the result of the model fitting using 6 experimental points with exponential coefficients. One can see that such a model does not predict unexplained changes in the stress value. For all the 8 experimental points, the result of model fitting with exponential coefficients is shown in Figure 2, f (green line). The results for the fitting parameters in the case of linear/exponential coefficients and for 6/8 experimental points are given in Table 3.

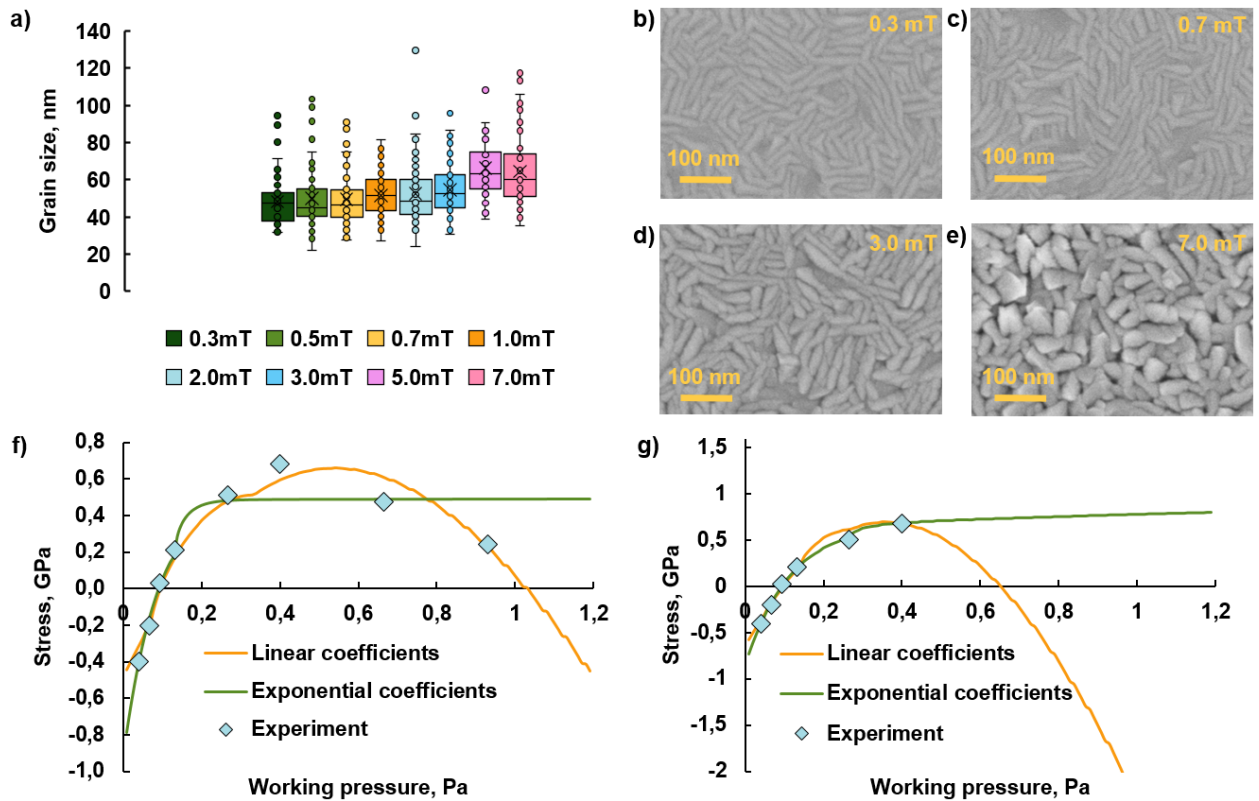


Figure 2. (a) Grain size dependence of Nb films on working pressure  $p_{Ar}$ . SEM images of Nb films deposited at  $p_{Ar}$  (b) 0.3 mTorr, (c) 0.7 mTorr, (d) 3.0 mTorr, (e) 7.0 mTorr. Results of the kinetic model approximation of the experimental dependence of stress in Nb films on the  $p_{Ar}$  for linear (orange line) and exponential (green line) coefficients for 8 points (f) and 6 points (g).



Table 3 - Values of the fitting parameters of the kinetic model for the cases of linear and exponential coefficients and 6 and 8 experimental points.

Coef.	$\sigma_t$ , GPa	$\sigma_c$ , GPa	$P_0$ , Pa	$\beta D_{eff}$ , nm <sup>2</sup> /s	$D_i$ , nm <sup>2</sup> /s	$A^*$ , GPa	$B^*$ , GPa	$l^*$ , nm	$p^*$
lin. 8	0.62	-18.67	0.33	0.08	3.19	-7.34	-0.96	3.55	-
exp. 8	0.50	-1.00	0.42	0.12	2.55	-7.72	-1.47	4.00	0.06
lin. 6	1.08	-22.22	0.27	0.31	2.15	-9.83	-0.87	3.99	-
exp. 6	1.19	-11.80	0.38	0.63	0.28	-2.06	-2.88	2.59	0.03

The suggested kinetic model with exponential coefficients allows improving the approximation error from 20 to 8%.

#### 4. Discussion

We have shown that the key parameter of magnetron sputtering in niobium thin films deposition is the argon working pressure ( $p_{Ar}$ ). The dependence of film roughness  $R_q$  on  $p_{Ar}$  confirms the published data [22], [23], [20], which indicate that  $R_q$  changes insignificantly with increasing  $p_{Ar}$  up to a certain value of  $p_{Ar}$ . In this study, the roughness degraded dramatically at  $p_{Ar}$  greater than 3 mTorr. The resistivity of Nb at low  $p_{Ar}$  is also almost constant, but at pressures above 2.0 mTorr it begins to increase. It is important to note that the scatter of resistivity values across the wafer also begins to increase at  $p_{Ar}$  greater than 2.0 mTorr. The roughness and resistivity data clearly indicate a degraded Nb film structure at  $p_{Ar}$  above 3.0 mTorr, which corresponds exactly to  $p_{critical}$ . It is well known that sputtered films contain Ar atoms due to a shot peening effect and the Ar content increases abruptly when  $p_{Ar}$  exceed certain thresholds. These threshold pressures coincide with the pressures where the tensile stress is maximum, i.e.  $p_{critical}$  [29], [55]. Ar content increasing causes to the porous microstructure observed by cross-sectional SEM [56]. As a result, the  $R_q$  and resistivity increase. These results may be important for other metals with low mobility for different applications, such as molybdenum [57], [58].

The dependence of stress in Nb films on  $p_{Ar}$  provides important information. This type of dependence, in whole or in part, is often found in scientific publications [22], [23], [28], [29]. However, it has not been demonstrated together with the dependence of resistivity on  $p_{Ar}$ . If we compare these two behaviors, it is obvious that when  $p_{critical}$  is exceeded the stress relaxes and the resistivity increases. According to the Mayadas–Shatzkes' grain boundary scattering model, an increase in resistivity means an increase the grain boundary reflection coefficient and indicates structural defects in the film [59], [34]. A similar dependence of the stress, structure, and morphology of the Nb film on the cathodic voltage during magnetron sputtering is shown in [29]. Thus, zero stress can be obtained in the range of small  $p_{Ar}$  and large  $p_{Ar}$ , but in the second case, the structure and morphology of the film are degraded (like dendritic-like structure in work [60]), and this degradation begins along with the relaxation of stress in the film.

The sputtering power in the range from 250– 400 W had no noticeable effect on the roughness and resistivity. This means that the critical power value below which the film structure degrades [29] did not fall within the investigated  $P_{sput}$  range.

Cryogenic characterization of Nb structures shows that RRR and  $T_C$  increase with increasing  $P_{\text{sput}}$ , which is in agreement with literature data [25], [29] and may be associated with a decrease in the  $\omega$ -phase content in the film [61]. The dependence of RRR and  $T_C$  on  $p_{\text{Ar}}$  is very indicative, where for  $p_{\text{Ar}}$  0.3, 0.7, 1.0 and 2.0 mTorr, RRR and  $T_C$  are almost the same. However, as  $p_{\text{Ar}}$  surpasses  $p_{\text{critical}}$ , the values of RRR and  $T_C$  decrease. The degraded cryogenic parameters of the Nb structures also confirm the degraded structure of the Nb films deposited at  $p_{\text{Ar}}$  above  $p_{\text{critical}}$ . The RRR value quantifies the overall level of impurities in niobium including: oxygen, nitrogen, hydrogen and argon [62], [63], so RRR decreasing confirms argon content increasing in a film. It is worth noting that the influence of stress in Nb films on the parameters of Nb films and Nb structures is insignificant if  $p_{\text{Ar}}$  is below  $p_{\text{critical}}$ , i.e.,  $p_{\text{Ar}}$  is on the left branch of the working pressure-stress graph. We assume that when the  $p_{\text{critical}}$  is exceeded, the film is not actually continuous, since internal stress relaxes due to plastic deformations and argon content in a film increases. As a result, all film parameters degraded.

The introduction of exponential coefficients to determine  $A_0$ ,  $B_0$ , and  $l_0$  into the kinetic model does not allow us to describe the relaxation of stress after exceeding  $p_{\text{critical}}$  value. However, our characterization data on Nb films and structures show that films at high  $p_{\text{Ar}}$  contain significant structural defects and cannot be considered continuous, even if they appear so in SEM images. In other words, the kinetic model is not applicable to films formed at  $p_{\text{Ar}}$  values above  $p_{\text{critical}}$ . For  $p_{\text{Ar}}$  less than  $p_{\text{critical}}$ , it is more physical to use exponential coefficients that reduce the high-energy terms of the kinetic model asymptotically to zero.

## 5. Conclusion

We have performed a comprehensive study of the influence of magnetron sputtering parameters on the niobium films and structures properties on  $\text{SiO}_2$  at room and cryogenic temperatures. We provided the experimentally obtained relationship between the mechanical, electrical, and cryogenic characteristics of the Nb films. We have shown that for Nb films, the key parameter of magnetron sputtering is the working pressure. We found critical working pressure  $p_{\text{critical}}$  above which (3.0 mTorr in our case), the intrinsic tensile stress starts to relax, but the roughness and resistivity increase whereas the residual resistance ratio RRR and the superconducting transition temperature  $T_C$  decrease. Below  $p_{\text{critical}}$  it is possible to control change of intrinsic stress in 200-nm Nb-film in the range from compression 400 MPa to tensile 600 MPa while maintaining perfect for SFQ-circuits parameters of the films: roughness  $R_q$  less than 0.8 nm, electrical resistivity less than  $20 \mu\Omega \times \text{cm}$ ,  $T_C$  more than 8.9 K and RRR more than 6.4. We have shown that the stress level in Nb films under the sputtering mode with fixed sputtering power  $P_{\text{sput}}$  remains constant throughout the target lifetime. We found that maximizing  $P_{\text{sput}}$  is necessary to increase RRR, and  $T_C$ . Finally, we used a kinetic model to predict the stress in Nb films and reduced the approximation error from 20 to 8% by replacing the linear dependence of the high-energy terms on the working pressure with an exponential one in it.

## **Declaration of Competing Interest**

The authors declare that they have no known competing financial interests or personal relationships that could have appeared to influence the work reported in this paper.

## **Acknowledgements**

Technology was developed and samples were fabricated at the BMSTU Nanofabrication Facility (Functional Micro/Nanosystems, FMNS REC, ID 74300).

## **Author contributions statement**

**EVZ:** Conceptualization (equal); Formal analysis (lead); Methodology (lead); Investigation (lead); Writing – original draft (lead); Visualization (lead).

**IAS:** Methodology (equal); Investigation (equal); Writing – review and editing (equal), visualization (supporting).

**SVB:** Methodology (equal); Investigation (equal).

**DAB:** Methodology (equal); Investigation (equal).

**MIT:** Methodology (equal); Investigation (equal).

**EAK:** Investigation (supporting); Writing – review and editing (equal).

**NSS:** Investigation (supporting); Writing – review and editing (equal).

**IAR:** Methodology (supporting); Writing – review and editing (supporting).

**SPB:** Formal analysis (supporting); Investigation (supporting).

**SAK:** Formal analysis (supporting); Investigation (supporting).

**NDK:** Methodology (supporting); Investigation (supporting).

**JAA:** Methodology (supporting); Investigation (supporting).

**IR:** Conceptualization (lead); Writing – review and editing (lead); Supervision (lead).

## **References**

[1] Likharev, Konstantin K. "Superconductor digital electronics." *Physica C*. 482 (2012): 6-18.

[2] Soloviev, Igor I., et al. "Beyond Moore's technologies: operation principles of a superconductor alternative." *Beilstein J. Nanotechnol.* 8.1 (2017): 2689-2710.

[3] Tolpygo, Sergey K. "Superconductor digital electronics: Scalability and energy efficiency issues." *Low Temp. Phys.* 42.5 (2016): 361-379.

- [4] Neilo, Alexey, et al. "Josephson spin valve controlled by a superconducting trigger effect." *Appl. Phys. Lett.* 125.16 (2024).
- [5] McDermott, Robert, et al. "Quantum–classical interface based on single flux quantum digital logic." *Quantum Sci. Technol.* 3.2 (2018): 024004.
- [6] Leonard Jr, Edward, et al. "Digital coherent control of a superconducting qubit." *Phys. Rev. Appl.* 11.1 (2019): 014009.
- [7] Castellanos-Beltran, M. A., et al. "Coherence-limited digital control of a superconducting qubit using a Josephson pulse generator at 3 K." *Appl. Phys. Lett.* 122.19 (2023).
- [8] Liu, Chuan-Hong, et al. "Single flux quantum-based digital control of superconducting qubits in a multichip module." *PRX Quantum* 4.3 (2023): 030310.
- [9] Koshelets, Valery P., et al. "An integrated 500 GHz receiver with superconducting local oscillator." *IEEE Trans. Appl. Supercond.* 7.2 (1997): 3589-3592.
- [10] Perelshtein, M. R., et al. "Broadband continuous-variable entanglement generation using a Kerr-free Josephson metamaterial." *Phys. Rev. Appl.* 18.2 (2022): 024063.
- [11] Benz, Samuel P. "Superconductor-normal-superconductor junctions for programmable voltage standards." *Appl. Phys. Lett.* 67.18 (1995): 2714-2716.
- [12] Schulze, H., et al. "Nb/Al/AIO<sub>x</sub>/AlO<sub>x</sub>/Al/Nb Josephson junctions for programmable voltage standards." *Appl. Phys. Lett.* 73.7 (1998): 996.
- [13] Fagaly, R. L. "Superconducting quantum interference device instruments and applications." *Rev. Sci. Instrum.* 77.10 (2006).
- [14] Tsoy, Georgiy, et al. "High-resolution SQUID magnetometer." *Physica B.* 284 (2000): 2122-2123.
- [15] Tolpygo, Sergey K., et al. "Advanced fabrication processes for superconducting very large-scale integrated circuits." *IEEE Trans. Appl. Supercond.* 26.3 (2016): 1-10.
- [16] Nagasawa, Shuichi, et al. "Nb 9-layer fabrication process for superconducting large-scale SFQ circuits and its process evaluation." *IEICE Trans. Electron.* 97.3 (2014): 132-140.
- [17] Abelson, Lynn A., and George L. Kerber. "Superconductor integrated circuit fabrication technology." *Proc. IEEE* 92.10 (2004): 1517-1533.
- [18] Altoé, M. Virginia P., et al. "Localization and mitigation of loss in niobium superconducting circuits." *PRX Quantum* 3.2 (2022): 020312.
- [19] Zikiy, E. V., et al. "High-Q trenched aluminum coplanar resonators with an ultrasonic edge microcutting for superconducting quantum devices." *Sci. Rep.* 13.1 (2023): 15536.
- [20] Du, Jia, Andrew DM Charles, and Karl D. Petersson. "Study of the surface morphology of Nb films and the microstructure of Nb/AlO<sub>x</sub>-Al/Nb trilayers." *IEEE Trans. Appl. Supercond.* 17.2 (2007): 3520-3524.

- [21] Kang, Xinjie, et al. "Growth and characterization of Nb films and Nb/Al-AIO x/Nb trilayers for Josephson junctions." *2013 IEEE 14th International Superconductive Electronics Conference (ISEC)*. IEEE, 2013.
- [22] Wu, Yu, et al. "Film stress influence on Nb/Al-AIOx/Nb Josephson junctions." *IEEE Trans. Appl. Supercond.* 29.5 (2019): 1-5.
- [23] Ying, Liliang, et al. "Development of multi-layer fabrication process for SFQ large scale integrated digital circuits." *IEEE Trans. Appl. Supercond.* 31.5 (2021): 1-4.
- [24] Xu, Qin-Yin, et al. "Fabrication of high-quality niobium superconducting tunnel junctions." *Chin. Phys. Lett.* 28.8 (2011): 087403.
- [25] Knappe, S., C. Elster, and H. Koch. "Optimization of niobium thin films by experimental design." *J. Vac. Sci. Technol.* 15.4 (1997): 2158-2166.
- [26] Kuroda, Kenichi, and Masahiro Yuda. "Niobium-stress influence on Nb/Al-oxide/Nb Josephson junctions." *J. Appl. Phys.* 63.7 (1988): 2352-2357.
- [27] Liu, Jianshe, et al. "Study of stress and morphology of superconducting niobium thin films." *IEEE Trans. Appl. Supercond.* 19.3 (2009): 245-248.
- [28] Meng, Xiaofan, et al. "Micron and submicron Nb/Al-AIO/sub x/Nb tunnel junctions with high critical current densities." *IEEE Trans. Appl. Supercond.* 11.1 (2001): 365-368.
- [29] Imamura, Takeshi, Tetsuyoshi Shiota, and Shinya Hasuo. "Fabrication of high quality Nb/AIO/sub x/-Al/Nb Josephson junctions. I. Sputtered Nb films for junction electrodes." *IEEE Trans. Appl. Supercond.* 2.1 (2002): 1-14.
- [30] Stepanov, Ilya A., et al. "Sputtered NbN films for ultrahigh performance superconducting nanowire single-photon detectors." *APL Mater.* 12.2 (2024).
- [31] Tolpygo, Sergey K., et al. "Advanced fabrication processes for superconductor electronics: Current status and new developments." *IEEE Trans. Appl. Supercond.* 29.5 (2019): 1-13.
- [32] Rodionov, Ilya A., et al. "Quantum engineering of atomically smooth single-crystalline silver films." *Sci. Rep.* 9.1 (2019): 12232.
- [33] Baburin, Aleksandr S., et al. "Evolutionary selection growth of silver films for low-loss nanophotonic devices." *Surf. Interfaces* 39 (2023): 102897.
- [34] Mayadas, A. F., M. Shatzkes, and J. F. Janak. "Electrical resistivity model for polycrystalline films: the case of specular reflection at external surfaces." *Appl. Phys. Lett.* 14.11 (1969): 345-347.
- [35] Holmes, D. Scott, and Jonathan McHenry. "Non-normal critical current distributions in Josephson junctions with aluminum oxide barriers." *IEEE Trans. Appl. Supercond.* 27.4 (2016): 1-5.
- [36] Premkumar, Anjali, et al. "Microscopic relaxation channels in materials for superconducting qubits." *Commun. Mater.* 2.1 (2021): 72.

- [37] Booi, Peter AA, Carol A. Livingston, and Samuel P. Benz. "Intrinsic stress in dc sputtered niobium." *IEEE Trans. Appl. Supercond.* 3.2 (1993): 3029-3031.
- [38] Amos, R. S., et al. "Stress and source conditions of DC magnetron sputtered Nb films." *IEEE Trans. Appl. Supercond.* 5.2 (1995): 2326-2329.
- [39] Iosad, N. N., et al. "Properties of DC magnetron sputtered Nb and NbN films for different source conditions." *IEEE Trans. Appl. Supercond.* 9.2 (1999): 1720-1723.
- [40] Abadias, Grégory, et al. "Stress in thin films and coatings: Current status, challenges, and prospects." *J. Vac. Sci. Technol. A* 36.2 (2018).
- [41] Koch, R. "Stress in evaporated and sputtered thin films—a comparison." *Surf. Coat. Technol.* 204.12-13 (2010): 1973-1982.
- [42] Janssen, G. C. A. M. "Stress and strain in polycrystalline thin films." *Thin solid films* 515.17 (2007): 6654-6664.
- [43] Chason, E., et al. "Kinetic model for dependence of thin film stress on growth rate, temperature, and microstructure." *J. Appl. Phys.* 111.8 (2012).
- [44] Chason, Eric. "A kinetic analysis of residual stress evolution in polycrystalline thin films." *Thin Solid Films* 526 (2012): 1-14.
- [45] Chason, E., et al. "A kinetic model for stress generation in thin films grown from energetic vapor fluxes." *J. Appl. Phys.* 119.14 (2016).
- [46] Su, Tong, et al. "Analysis of stress in sputter-deposited films using a kinetic model for Cu, Ni, Co, Cr, Mo, W." *Appl. Surf. Sci.* 613 (2023): 156000.
- [47] Chason, Eric, et al. "Kinetic model for thin film stress including the effect of grain growth." *J. Appl. Phys.* 123.18 (2018).
- [48] Chaudhari, P. "Grain growth and stress relief in thin films." *J. Vac. Sci. Technol.* 9.1 (1972): 520-522.
- [49] Thornton, John A., and D. W. Hoffman. "Stress-related effects in thin films." *Thin solid films* 171.1 (1989): 5-31.
- [50] Magnfält, Daniel, et al. "Compressive intrinsic stress originates in the grain boundaries of dense refractory polycrystalline thin films." *J. Appl. Phys.* 119.5 (2016).
- [51] Chason, Eric, and Pradeep R. Guduru. "Tutorial: Understanding residual stress in polycrystalline thin films through real-time measurements and physical models." *J. Appl. Phys.* 119.19 (2016).
- [52] Johnson, Jonathan A., et al. "Inter-relationship of stress and microstructure in BCC and 'beta'tungsten films." *Surf. Coat. Technol.* 457 (2023): 129336.
- [53] Rao, Zhaoxia, et al. "Understanding residual stress in thin films: Analyzing wafer curvature measurements for Ag, Cu, Ni, Fe, Ti, and Cr with a kinetic model." *J. Appl. Phys.* 130.13 (2021).

[54] Mattox, D. M., and R. E. Cuthrell. "Residual stress, fracture, and adhesion in sputter-deposited Molybdenum films." *MRS Online Proceedings Library* 119 (1988): 141-146.

[55] Wu, C. T. "Intrinsic stress of magnetron-sputtered niobium films." *Thin Solid Films* 64.1 (1979): 103-110.

[56] Imamura, Takeshi, and Shinya Hasuo. "Effects of intrinsic stress on submicrometer Nb/AlO<sub>2</sub>/Nb Josephson junctions." *IEEE Trans. Magn.* 25.2 (1989): 1119-1122.

[57] Ahmed, Nisar, Zuhair S. Khan, and Asghar Ali. "Microstructure and residual stress dependence of molybdenum films on DC magnetron sputtering conditions." *Appl. Phys. A.* 128.11 (2022): 967.

[58] Konstantinova, T. G., et al. "Deep multilevel wet etching of fused silica glass microstructures in BOE solution." *Sci. Rep.* 13.1 (2023): 5228.

[59] Zhang, Wenqi, et al. "Influence of the electron mean free path on the resistivity of thin metal films." *Microelectron. Eng.* 76.1-4 (2004): 146-152.

[60] Shen, Y. G. "Effect of deposition conditions on mechanical stresses and microstructure of sputter-deposited molybdenum and reactively sputter-deposited molybdenum nitride films." *Mater. Sci. Eng. A* 359.1-2 (2003): 158-167.

[61] Lee, Jaeyel, et al. "Stress-induced structural changes in superconducting Nb thin films." *Phys. Rev. Mater.* 7.6 (2023): L063201.

[62] Splett, Jolene D., Dominic F. Vecchia, and Loren F. Goodrich. "A comparison of methods for computing the residual resistivity ratio of high-purity niobium." *J. Res. Natl. Inst. Stand. Technol.* 116.1 (2011): 489.

[63] Krishnan, Mahadevan, et al. "Very high residual resistivity ratios of heteroepitaxial superconducting niobium films on MgO substrates." *Supercond. Sci. Technol.* 24.11 (2011): 115002.